

Article

Not peer-reviewed version

Optimizing Transmit Power for User-Cooperative Backscatter-assisted NOMA-MEC: A Green IoT Perspective

[Huaiwen He](#), Chenghao Zhou, Feng Huang, [Hong Shen](#), Yihong Yang, [Dengsheng Yu](#)^{*}, [Huimin Huang](#)^{*}

Posted Date: 23 October 2024

doi: 10.20944/preprints202410.1781.v1

Keywords: NOMA-MEC (non-orthogonal multiple access - mobile edge computing); wireless power transfer (WPT); Backscatter communication (Backcom); Lyapunov optimization; transmit power



Preprints.org is a free multidiscipline platform providing preprint service that is dedicated to making early versions of research outputs permanently available and citable. Preprints posted at Preprints.org appear in Web of Science, Crossref, Google Scholar, Scilit, Europe PMC.

Copyright: This is an open access article distributed under the Creative Commons Attribution License which permits unrestricted use, distribution, and reproduction in any medium, provided the original work is properly cited.

Disclaimer/Publisher's Note: The statements, opinions, and data contained in all publications are solely those of the individual author(s) and contributor(s) and not of MDPI and/or the editor(s). MDPI and/or the editor(s) disclaim responsibility for any injury to people or property resulting from any ideas, methods, instructions, or products referred to in the content.

Article

Optimizing Transmit Power for User-Cooperative Backscatter-Assisted NOMA-MEC: A Green IoT Perspective

Huaiwen He ¹, Chenghao Zhou ^{1,2}, Feng Huang ^{1,2}, Hong Shen ³, Yihong Yang ¹, Dengsheng Yu ^{4,*} and Huimin Huang ^{4,*}

¹ School of Computer, Zhongshan Institute, University of Electronic Science and Technology of China, Zhongshan 528400, China

² Computer Science and Engineering School, University of Electronic Science and Technology of China, Chengdu 611731, China

³ School of Engineering and Technology, Central Queensland University, Rockhampton 4701, Australia

⁴ Wenzhou University of Technology, Wenzhou, China

* Correspondence: yudengsheng@126.com (D.Y.); huanghm27@mail2.sysu.edu.cn (H.H.)

Abstract: Non-orthogonal multiple access (NOMA) enables the parallel offloading of multiuser tasks, effectively enhancing throughput and reducing latency. Backscatter communication, which passively reflects radio frequency (RF) signals, improves energy efficiency and extends the operational lifespan of terminal devices. Both technologies are pivotal for the next generation of wireless networks. However, there is little research focusing on optimizing the transmit power in backscatter-assisted NOMA-MEC systems from a green IoT perspective. In this paper, we aim to minimize the transmit energy consumption of a Hybrid Access Point (HAP) while ensuring task deadlines are met. We consider the integration of Backscatter Communication (BackCom) and Active Transmission (AT), and leverage NOMA technology and user cooperation to mitigate the double near-far effect. Specifically, we formulate a transmit energy consumption minimization problem, accounting for task deadline constraints, task offloading decisions, transmit power allocation, and energy constraints. To tackle the non-convex optimization problem, we employ variable substitution and convex optimization theory to transform the original non-convex problem into a convex one, which is then efficiently solved. We deduce the semi-closed form expression of the optimal solution and propose an energy-efficient algorithm to minimize the transmit power of the entire wireless powered MEC. Simulation results demonstrate that our proposed scheme significantly reduces the transmit power of the HAP compared to existing schemes, validating the effectiveness of our approach. This study provides valuable insights for the design of green IoT systems by optimizing the transmit power in NOMA-MEC networks.

Keywords: NOMA-MEC (non-orthogonal multiple access - mobile edge computing); wireless power transfer (WPT); Backscatter communication (Backcom); Lyapunov optimization; transmit power

1. Introduction

The rapid development of the Internet of Things (IoT) has driven an increasing demand for efficient data processing and low-latency communication in mobile devices such as autonomous vehicles, facial recognition systems, virtual reality (VR) devices, and electronic health monitors [1,2]. To address the limitations in computational power and battery life of these devices, Mobile Edge Computing (MEC) technology offloads computationally intensive tasks to servers deployed at the network's edge, such as base stations, thereby effectively enhancing the devices' computational capacity and response speed [3,4]. Additionally, Wireless Power Transmission (WPT) [5] technology collects energy remotely through radio frequency (RF) signals, further extending the battery life of devices. Leveraging the advantages of MEC and WPT networks, numerous studies have been conducted to explore the potential of Wireless-Powered MEC (WPMEC) systems, and a multitude of efficient algorithms have been proposed to address the joint allocation of communication and computational resources.

However, to address the challenges of serving the massive number of devices in future wireless networks, relying solely on MEC may not suffice to meet service demands. Beyond computational and

battery limitations, the double near-far effect can severely impact network performance, particularly for devices far from the Hybrid Access Point (HAP) and often facing poor channel conditions [6]. To overcome these challenges, researchers have proposed a collaborative computing model [7]. This model activates underutilized computational resources within the network, allowing nearby users to assist distant users in offloading computational tasks, thereby improving data transmission rates under unfavorable channel conditions and enhancing the overall performance of the system. This approach not only increases the efficiency with which distant users offload tasks to access points but also makes full use of idle computing resources in the network through Device-to-Device (D2D) [8,9] communication and User Collaboration (UC) [10–12] mechanisms, optimizing resource allocation, effectively improving energy efficiency, and addressing the challenges posed by geographical disparities.

The integration of Non-Orthogonal Multiple Access (NOMA) technology into WPMEC systems has been identified as a means to enhance overall performance [13,14]. This approach allows for the shared use of time-frequency resources among users, leveraging power domain multiplexing and multi-user detection techniques such as Successive Interference Cancellation (SIC) [15]. The adoption of these techniques not only improves spectral efficiency but also substantially increases system capacity and coverage, which is particularly beneficial in frequency-constrained or densely populated urban scenarios.

Backscatter Communication (BackCom) technology has emerged as a promising approach in mobile communication due to its low energy footprint [10,16–20]. This technology facilitates the transmission of information through the passive reflection of radio frequency signals, concurrently harvesting energy to power circuit operations. When compared to the traditional active transmission (AT) model, which follows the Harvest-then-Transmit (HTT) protocol, BackCom dramatically minimizes energy usage, typically requiring only a few microwatts to hundreds of microwatts, despite offering comparatively lower transmission rates. To optimize the trade-off between energy harvesting and data transmission, and to concurrently enhance system throughput and energy efficiency (EE) [21], BackCom can be strategically combined with AT. This dual-mode approach capitalizes on the complementary strengths of both communication methods.

While extensive research [22–26] has explored the use of BackCom and NOMA to improve the efficiency of wireless spectrum utilization and wireless energy transfer, there is a lack of studies investigating the synergistic application of BackCom and NOMA in scenarios involving user cooperation. Additionally, the majority of existing work on energy optimization in WPMEC systems has focused on energy consumption at the mobile device (MD) level. However, since the energy for MDs is entirely harvested from the RF signals emitted by the HAP, the energy transmitted by the HAP constitutes the total energy budget of the WPMEC system. Therefore, optimizing the energy consumption of HAP transmissions is of significant practical importance.

In this paper, we consider a transmit energy minimization (TEM) problem for a UC-based wireless powered NOMA-MEC network, integrating BackCom and AT communication modes. We jointly optimize the WPT time fraction, backscatter time fraction, task offloading time fraction, transmit power allocation of the MD node, and backscatter reflection coefficients, aiming to minimize the total transmit power of the HAP while meeting task latency constraints. We formulate the mathematical model for the TEM problem, which is strongly non-convex. Due to signal interference in NOMA communication, there is a coupling between transmission power allocation decisions, and the coupling between BackCom communication and AC communication introduces additional coupling in the offloading of data, posing significant challenges in solving the problem. To address this highly non-convex TEM problem, we employ variable substitution techniques and convex optimization theory to convert it into a convex problem, allowing for efficient solutions. Extensive numerical simulations are conducted to verify the performance and effectiveness of our proposed scheme.

The primary contributions are summarized as follows:

- Proposing an innovative energy optimization model for a WPMEC system from a green IoT perspective. We formulate a TEM problem for HAP under task delay constraints, while leveraging

the NOMA technique, integrating BackCom with AT communication, and employing user cooperation to alleviate the impact of the double near-far effect. Furthermore, our model focuses on the optimization of the overall energy consumption in WPMEC networks, rather than solely considering the energy expenditure of mobile nodes. The model has practical application value for reducing carbon emissions in WPMEC and promoting the development of green IoT technologies.

- Applying variable substitution and convex optimization theory to convert the non-convex TEM problem into a convex one. Through a meticulous analysis of the problem's structure, we have developed a low-complexity algorithm to solve it and derived a semi-closed-form expression for the optimal solution.
- Evaluating the performance of our scheme through extensive simulations. The experimental results demonstrate that our proposed scheme surpasses the state-of-the-art methods, with an approximate improvement of 8%.

The remainder of this paper is organized as follows: Section II provides an overview of the related works in the field. In Section III, we details the model of the Backscatter-Aided wireless powered NOMA-MEC system. In Section IV, formulates the transmit power optimization problem, presenting the mathematical formulation. Section V, we develop a low-complexity algorithm designed to solve the optimization problem. Section V offers a comprehensive evaluation of the proposed algorithm's performance through extensive simulations. In Section VI, we conclude the paper by summarizing the key findings and contributions, and suggest potential directions for future research.

2. Related Work

In order to increase the data computation capability and decrease the task processing delay, the resource management in WPT assisted MEC network has been extensively studied [27]. Zhang *et al.* [28] presents a mobility-aware hierarchical MEC framework for IoT, employing a game theoretic approach to enhance energy efficiency and reduce latency in computation offloading. Dinh *et al.* [29] introduces a semidefinite relaxation (SDR)-based approach for task offloading from a mobile device to multiple edge devices, aiming to minimize execution latency through joint task allocation and CPU frequency optimization in both fixed and elastic CPU frequency scenarios. Moreover, energy consumption as a determining factor of network performance has been widely explored in MEC networks. Wang *et al.* [30] proposes a modified-cutting-plane (MCP) algorithm and a pivoting-and-subgradient (PS) algorithm to minimize total energy consumption in a multi-cell MEC system. Mei *et al.* [31] explores a dynamic energy-efficient task offloading algorithm for a multi-device single-MEC system, leveraging Lyapunov optimization to minimize energy consumption while maintaining system stability. Chen *et al.* [32] introduces a polling callback energy-saving offloading strategy for MEC systems to address asynchronous data transmission and task processing times, and employs a game-learning algorithm combining DDQN and distributed LSTM to optimize energy consumption. However, prior researches have not accounted for the dynamic network conditions, such as stochastic task arrivals and variable wireless channel states.

For energy-efficient and low-latency task offloading, a variety of innovative technologies, especially BackCom and NOMA, have been leveraged in MEC networks [33,34]. Toro *et al.* [35] provides a comprehensive survey on BackCom for green IoT, examining its operating principles, applications in various domains, and addressing operational and security challenges. Shi *et al.* [36] introduces a hybrid approach combining Harvest-Then-Transmit (HTT) with Backscatter communication aimed at maximizing the weighted sum of computation bits within a WPT-MEC network, taking into account a realistic non-linear energy harvesting (EH) model. Additionally, Khan *et al.* [34] explores the integration of 6G communications, specifically NOMA and Backcom, to enhance energy efficiency and data sharing in Automotive Industry 5.0, proposing a multicell optimization framework for backscatter-enabled NOMA vehicular networks. Fang *et al.* [37] proposes an energy-efficient optimization scheme for a multi-user NOMA-MEC network, employing a bilevel programming method to derive optimal

solutions for a one-user two-base station (BS) scenario and extends it to a low-complexity algorithm for the multi-user and multi-BS case. Shi *et al.* [38] presents a NOMA-based millimeter-wave (mmW) MEC mechanism to minimize the average delay of MEC offloading by jointly optimizing beamwidth, user equipment scheduling, and transmit power, employing alternative optimization and matrix control algorithms to enhance accessing efficiency.

Researchers have extensively adopted user cooperation mechanism to mitigate the double-near-far effect and optimize resource utilization in MEC systems [39–41]. Sun *et al.* [39] introduces an iterative algorithm designed to minimize end-to-end latency in IoT environment, jointly optimizing user association and resource allocation in a three-phase operation protocol. Lyu *et al.* [40] considered user-cooperation schemes in different communication modes, Backscatter and HTT, improving network communication capability and energy efficiency by optimizing time and power allocation and energy beamforming. Li *et al.* [11] employs a multi-user cooperation scheme to enhance computation performance in a WPMEC system, focusing on maximizing the weighted sum computation rate by jointly optimizing collaboration, time, and data allocation among IoT devices and an HAP. Huang *et al.* [41] introduces a NOMA-assisted cooperative computing scheme with user cooperation in a three-node MEC system to leverage idle mobile device resources, optimizing energy consumption and offloading data through joint communication and computation resource allocation. Our previous research [7] addresses the challenge of energy management in WPT-MEC networks with user cooperation by proposing a multi-stage stochastic optimization approach, introducing Lyapunov optimization technique to ensure sustainability and stability in the dynamic IoT environment. However, the integration of BackCom and NOMA in user collaboration systems remains unexplored in the aforementioned work.

3. System Model

3.1. Communication Model

We consider a user-cooperative wireless-powered MEC system, comprising a user node, a helper node, and a HAP, as illustrated in Figure 1. The HAP is equipped with an RF energy transmitter and is directly connected to an edge server. The user node, denoted as MD₁, is located at a greater distance from the HAP, while the helper node, MD₂, is positioned closer to the HAP. Both MD₁ and MD₂ have individual computation tasks that must be completed within a specified latency constraint. Additionally, both nodes are equipped with a BackCom circuit and an AT circuit, allowing them to select between backscatter communication and active communication modes.

In this three-node model, both MD₁ and MD₂ have their own data processing tasks with data-size L_1 and L_2 that need to be completed within a specified time T . MD₁ is positioned between MD₂ and the HAP, allowing it not only to process its own data but also to assist MD₂ in relaying data offloaded to the edge server. The system employs a NOMA communication scheme, which allows MD₂ to offload data simultaneously to both MD₁ and the HAP. We focus on a zero-power IoT system, where the energy for mobile nodes MD₁ and MD₂ is entirely derived from wireless power transfer by the HAP. By using wireless charging, MD₁ and MD₂ eliminate the additional costs associated with battery replacement.

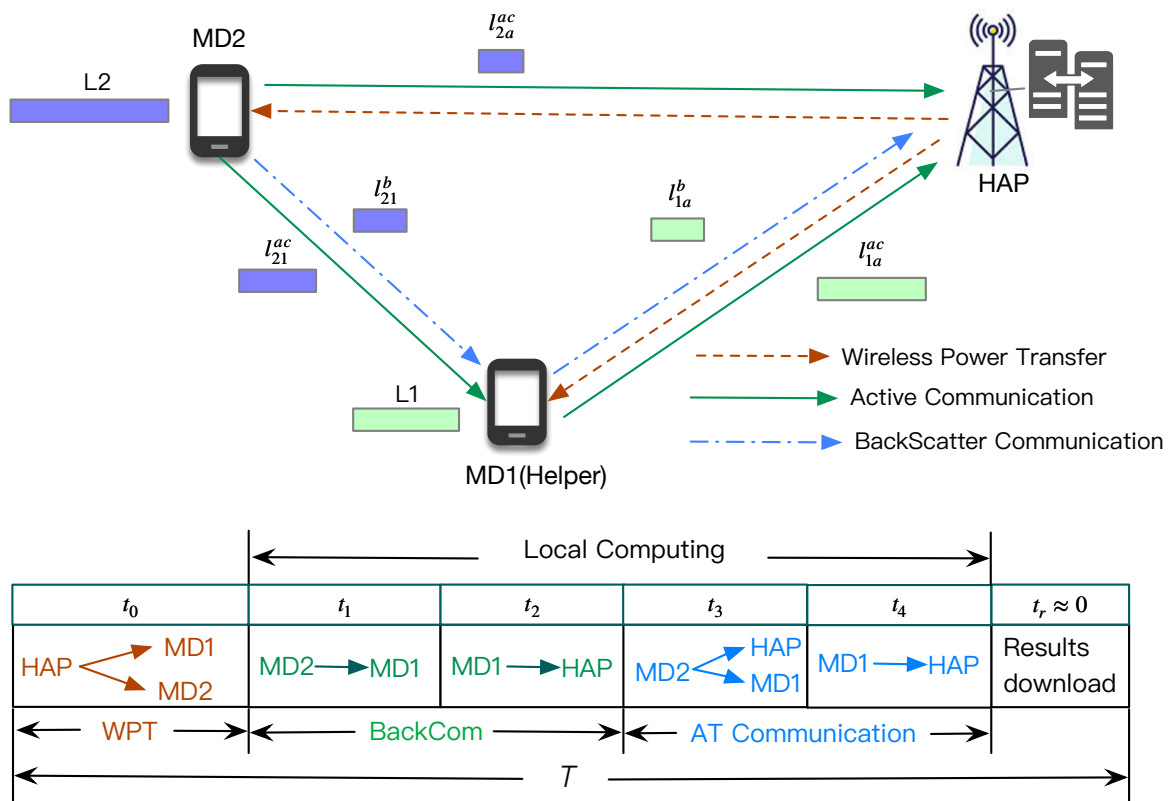


Figure 1. System model of WPMEC network with user-assisted

The system adopts a partial offloading model, allowing computational tasks to be fragmented and offloaded to the edge server. The communication process of the system is as follows: Initially, at time t_0 , MD₁ and MD₂ receive wireless energy transmitted by the HAP's RF equipment, which is used to process their respective computational tasks, denoted as L_1 and L_2 . Since the system employs a hybrid transmission mode combining BackCom and AC, data offloading begins with BackCom. At time t_1 , MD₂ partially offloads its data to MD₁ using BackCom, with the offloaded data size denoted as l_{21}^b . Subsequently, during the t_2 time slot, MD₁ offloads its data to the HAP via BackCom, with the offloaded data size denoted as l_{1a}^b .

Next, task offloading proceeds using the AT mode. During the t_3 time slot, MD₂, utilizing NOMA technique, simultaneously offloads data to both MD₁ and the HAP, with data sizes denoted as l_{21}^{ac} and l_{2a}^{ac} , respectively. In the t_4 time slot, MD₁ offloads its data to the edge server connected to the HAP, with the offloaded data size denoted as l_{1a}^{ac} . Finally, during the t_r time slot, the computation results are downloaded from the edge server. because the computation result data is typically small, the time required for this step can be considered negligible.

The primary symbols and definitions used are listed in Table 1.

Table 1. KEY NOTATIONS AND DEFINITIONS

Notation	Definition
T	The time block
t_0	The time for WPT
$t_1 t_2$	The time for offloading by Backcom of MD ₂ and MD ₁
t_3, t_4	The time for offloading by AC of MD ₂ and MD ₁
L_i	the amount of computational tasks of MD ₁ and MD ₂
h_i	The WPT channel gain between MD _i and HAP
g_{12}, g_{2a}	The offloading channel gain between MD ₁ and MD ₂ , MD ₂ and HAP
P_0, P_1, P_{21}, P_{2a}	The transmit power by AC at HAP, MD ₁ and MD ₂
P_i^b	The circuit power by Backcom at MD _i
l_i^{loc}	The amount of tasks processed locally at MD _i
l_{1a}^b, l_{21}^b	The amount of tasks offloaded by Backcom at MD ₁ and MD ₂
$l_{1a}^{ac}, l_{2a}^{ac}, l_{21}^{ac}$	The amount of tasks offloaded by AC at MD ₁ and MD ₂
e_i^{loc}	The energy consumed by processing tasks locally at MD _i
e_i^b	The energy consumed by offloading tasks by Backcom at MD _i
f_i	The local CPU frequency at MD _i
ϕ_i	The CPU cycles required to compute one bit task at MD _i
β_i^t	The reflection coefficient of MD _i at slot t
μ	The energy conversion efficiency
κ_i	The computing energy efficiency of MD ₁ and MD ₂
B	The channel bandwidth
σ^2	The additive white Gaussian noise

3.2. Wireless Powered Transfer Model

During both the WPT charging phase and the BackCom communication phase, the MD can harvest RF energy from the HAP's RF transmitter. This harvested energy is used for both local computation and task offloading. Let P_0 denote the RF transmit power of the HAP, and μ ($0 < \mu < 1$) represents the energy conversion efficiency. The amount of harvested energy of MD₂ is given by [10]:

$$E_2 = \mu h_2 P_0 (t_0 + t_2) \quad (1)$$

where h_2 represents the channel gain from the HAP to MD₁, which remain constant within the T time period. Similar, the amount of harvested energy of MD₁ is as

$$E_1 = \mu h_1 P_0 (t_0 + t_1) \quad (2)$$

where h_1 represents the channel gain from the HAP to MD₁

3.3. Computing Model

Upon the arrival of a task at a mobile node, a portion of the task may be offloaded to the edge server, while the remaining part is processed locally. Let the CPU frequencies of MD₁ and MD₂ be denoted as f_1 and f_2 , respectively, and let the number of CPU cycles required to process one bit of data be represented by ϕ_1 and ϕ_2 . The amount of task data processed locally at MD₂ is $(L_2 - l_{21}^b - l_{2a}^{ac} - l_{21}^{ac})$. Thus, the corresponding energy consumption for local computing can be expressed as [10]

$$e_2^{loc} = \kappa_2 (L_2 - l_{21}^b - l_{2a}^{ac} - l_{21}^{ac}) \phi_2 (f_2)^2 \quad (3)$$

where κ_2 represents the computing energy efficiency parameter of MD₂ [10].

The local computing latency constraint for MD₂ is

$$\frac{(L_2 - l_{21}^b - l_{2a}^{ac} - l_{21}^{ac})\phi_2}{f_2} \leq T - t_0 \quad (4)$$

For MD₁, which is responsible for forwarding MD₂'s data to HAP without performing local computation on MD₂'s data. Therefore, we have the following data constraint:

$$l_{1a}^b + l_{1a}^{ac} \geq l_{21}^b + l_{21}^{ac} \quad (5)$$

Similarly, the amount of task data that is processed locally on MD₁ is equal $L_1 + l_{21}^b + l_{21}^{ac} - l_{1a}^b - l_{1a}^{ac}$, and the energy consumption for local computing at MD₁ is

$$e_1^{loc} = \kappa_1(L_1 + l_{21}^b + l_{21}^{ac} - l_{1a}^b - l_{1a}^{ac})\phi_1(f_1)^2 \quad (6)$$

where κ_1 denotes the computing energy efficiency parameter of MD₁ [10].

The local computing latency constraint for MD₂ is

$$\frac{(L_1 + l_{21}^b + l_{21}^{ac} - l_{1a}^b - l_{1a}^{ac})\phi_1}{f_1} \leq T - t_0 \quad (7)$$

where κ_i denotes the computing energy efficiency parameter of MD₁ [10].

3.4. Task Offloading Model

3.4.1. Offloading Task by BackCom

During t_1 time slot, MD₂ offload tasks to MD₁ by using Backscatter communication. We denote the reflection coefficient of BackCom at MD₂ as β_1 , $0 \leq \beta_2 \leq 1$, which plays a crucial role for a balance between energy harvesting and communication performance. Thus, there is β_1 proportion of energy utilized as a carrier to transfer data, and $(1 - \beta_1)$ proportion of incident power that is absorbed by MD₂ [17]. According to Shannon's theorem [42], the amount of tasks offloaded from MD₂ to MD₁ is as follows:

$$l_{21}^b = t_1 B \log_2 \left(1 + \frac{\zeta \beta_2 P_0 h_2 g_{21}}{\sigma^2} \right) \quad (8)$$

where ζ represents the performance gap reflecting real modulation of BackCom [18], g_{21} denotes the channel gain from MD₂ to MD₁, and σ^2 is the noise power.

The corresponding energy consumption for task offloading by BackCom is

$$e_2^b = P_2^b t_1 \quad (9)$$

where P_2^b is the circuit power consumption of MD₂ by BackCom, which is a constant value depending on the circuit structure. In BackCom communication, a node can simultaneously reflect the signal and harvest RF energy. The energy harvested by MD₂ during the BackCom communication at time t_1 is expressed as follows:

$$E_2^b = \mu h_2 P_0 t_1 (1 - \beta_2) \quad (10)$$

After receiving the tasks offloaded by MD₂, MD₁ will act as a relay and forward a portion of these tasks to the HAP. Additionally, MD₂ will offload its own tasks to the HAP. At time t_2 , the task data transmitted by MD₂ via BackCom is subject to the following constraints.

$$l_{1a}^b = t_2 B \log_2 \left(1 + \frac{\zeta \beta_1 P_0 h_1 g_{1a}}{\sigma^2} \right) \quad (11)$$

where β_1 is the reflection coefficient of the BackCom at MD₁, and g_{1a} represents the channel gain from MD₁ to the HAP. The corresponding energy consumption for task offloading by BackCom is

$$e_1^b = P_1^b t_2 \quad (12)$$

where P_2^b is the circuit power consumption of MD₂ by BackCom. The energy harvested of MD₁ by Backcom during t_2 is

$$E_1^b = \mu h_1 P_0 t_2 (1 - \beta_1) \quad (13)$$

3.4.2. Offloading Task by NOMA-Aided AC Communication

In the AC transfer mode, we adopt NOMA technique improve the task transmission efficiency. In time slot t_3 , MD₂ simultaneously offload task to MD₁ and the HAP with data size $l_{21}^{ac} \in \mathbb{R}_{\geq 0}$ and $l_{2a}^{ac} \in \mathbb{R}_{\geq 0}$, respectively. In the NOMA transmission process, the transmit allocation allocated for task offloading to MD₁ and the HAP are denoted as $p_{21} \in \mathbb{R}_{\geq 0}$ and $p_{2a} \in \mathbb{R}_{\geq 0}$. MD₂ transmits a linear superposition signal to MD₁ and the HAP. We suppose that the global channel state information (CSI) of network can be obtained. After receiving the signal, MD₁ first decodes the MD₂'s signal and subtracts it from the received signal by leveraging the successive interference cancellation (SIC) technique. By denoting the channel coefficients from MD₂ to MD₁ and the HAP as g_{21} and g_{2a} , respectively. Therefore, the task offloading rate from MD₂ to MD₁ and the HAP can be expressed as follows:

$$R_{21}^{ac} = B \log_2(1 + h_{21} p_{21}) \quad (14)$$

$$R_{2a}^{ac} = B \log_2 \left(1 + \frac{h_{2a} p_{2a}}{1 + h_{2a} p_{21}} \right) \quad (15)$$

where $h_{21} := |g_{21}|^2 / \sigma^2$ and $h_{2a} := |g_{2a}|^2 / \sigma^2$ represent the effective channel gain to the noise power ratio (ECG NR) from MD₂ to MD₁ and the HAP, respectively.

During the time slot t_3 , the amount of offloaded task from MD₂ offloading to MD₁ and the HAP are define to be

$$l_{21}^{ac} = R_{21}^{ac} t_3 \quad (16)$$

$$l_{2a}^{ac} = R_{2a}^{ac} t_3 \quad (17)$$

The energy consumption of task offloading from MD₂ to MD₁ and the HAP via NOMA are obtained as $p_{21} t_3$ and $p_{2a} t_3$.

At the t_4 time slot, MD₁ offloads computation task to HAP by utilizing the AC mode, which includes tasks offloaded from MD₂ and task native to MD₁. The amount of task offloading from MD₁ to the HAP is

$$l_{1a}^{ac} = t_4 B \log_2(1 + h_{1a} p_1) \quad (18)$$

where $0 \leq p_1^t \leq P_1^{\max}$ represents the transmit power allocated to AC at MD₁ [10]. $h_{1a} := |g_{1a}|^2 / \sigma^2$ represents ECG NR from MD₁ to the HAP, and g_{1a} is channel coefficients from MD₁ to the HAP.

The energy consumption for offloading task from MD₁ to the HAP is $P_1 t_4$.

4. Problem Formulation

In this paper, we consider to design computation task offloading algorithm to minimize the carbon footprint for a green IoT network with NOMA-Backscatter assisted under user cooperation. We make jointly decisions on time slot allocation $\mathbf{t} = [t_0, t_1, t_2, t_3, t_4]$, power allocation $\mathbf{p} = [p_{21}, p_{2a}, p_1]$, Backscatter reflection coefficients $\boldsymbol{\beta} = [\beta_1, \beta_2]$ and the size of offloading tasks $\mathbf{l} = [l_{21}^b, l_{1a}^b, l_{21}^{ac}, l_{2a}^{ac}, l_{1a}^{ac}]$ to minimize the total transmit power of HAP subjected to the common latency constraints. The HAP's transmit power minimization (TPM) problem can be defined as follows:

$$(P1) : \min_{t,p,\beta,l} P_0(t_0 + t_1 + t_2) \quad (19a)$$

$$\text{s.t. } t_0 + t_1 + t_2 + t_3 + t_4 \leq T, \quad (19b)$$

$$P_2^b t_1 + p_{21} t_3 + p_{2a} t_3 + e_2^{loc} \leq E_2 + E_2^b, \quad (19c)$$

$$P_1^b t_2 + p_1 t_4 + e_1^{loc} \leq E_1 + E_1^b, \quad (19d)$$

$$p_{21} + p_{2a} < P_2^{max}, \quad (19e)$$

$$p_1 \leq P_1^{max}, \quad (19f)$$

$$l_{21}^{ac} + l_{2a}^b \leq l_{1a}^b + l_{1a}^{ac}, \quad (19g)$$

$$\frac{(L_2 - l_{21}^b - l_{2a}^{ac} - l_{21}^{ac})\phi_2}{f_2} \leq T - t_0, \quad (19h)$$

$$\frac{(L_1 + l_{21}^b + l_{21}^{ac} - l_{1a}^b - l_{1a}^{ac})\phi_1}{f_1} \leq T - t_0, \quad (19i)$$

$$p \in \mathbb{R}_{\geq 0}, \beta \in \mathbb{R}_{\geq 0}, l \in \mathbb{R}_{\geq 0}, t \in \mathbb{R}_{\geq 0}, \quad (19j)$$

where constraint (19b) specifies the time slot allocation. Constraints (19c) and (19d) set the energy consumption limits for MD₂ and MD₁, respectively. Constraints (19e) and (19f) governs the transmit power allocation for both MD₂ and MD₁. Constraint (19g) ensures that the task offloaded from MD₂ to MD₁ is relayed to the HAP within the specified time T . Constraints (19h) and (19i) impose the task processing latency requirements for MD₂ and MD₁, respectively. Constraint (19j) defines the feasible domain for the decision variables.

Note that Problem (P1) is a non-convex optimization problem due to the nonconvex the objective function and nonconvex constraints (19c) and (19d). This characteristic precludes the use of traditional convex optimization methods for its direct solution. Therefore, through in-depth analysis of the problem's structure and careful design, we employ the variable substitutions to solve Problem P1.

5. Optimal Solution for the TPM Problem

Problem P1 remains a nonconvex optimization problem due to the nonconvexity of constraints (19c) and (19d), and the presence of the coupling decision variables p and l . To address this, we first rewrite p_{21} and p_{1a} based on equations (14) and (18) as follows:

$$p_{21} = \frac{1}{h_{21}} f\left(\frac{l_{21}^{ac}}{Bt_3}\right) \quad (20)$$

$$p_1 = \frac{1}{h_{1a}} f\left(\frac{l_{1a}^{ac}}{Bt_4}\right) \quad (21)$$

where the function f is define as $f : \mathbb{R} \rightarrow \mathbb{R}, x \mapsto 2^x - 1$ for all $x \in \mathbb{R}$.

Lemma 1. *The sum of the transmit power p_{21} and p_{2a} can be expressed as:*

$$p_{21} + p_{2a} = \frac{1}{h_{21}} f\left(\frac{l_{21}^{ac} + l_{2a}^{ac}}{Bt_3}\right) + \left(\frac{1}{h_{2a}} - \frac{1}{h_{21}}\right) f\left(\frac{l_{2a}^{ac}}{Bt_3}\right)$$

Proof. From equation (15), we have

$$\frac{p_{2a}}{1 + h_{2a} p_{21}} = \frac{1}{h_{2a}} f\left(\frac{l_{2a}^{ac}}{Bt_3}\right) \quad (22)$$

Substituting equation (20) into (22), we express p_{2a} as

$$p_{2a} = \frac{1}{h_{2a}} f\left(\frac{l_{2a}^{ac}}{Bt_3}\right) + \frac{1}{h_{2a}} f\left(\frac{l_{21}^{ac}}{Bt_3}\right) f\left(\frac{l_{2a}^{ac}}{Bt_3}\right) \quad (23)$$

Utilizing the identity $f(x_1) \cdot f(x_2) = f(x_1 + x_2) - f(x_1) - f(x_2)$, we can expand the right hand size of (24) as

$$p_{2a} = \frac{1}{h_{21}} f\left(\frac{l_{21}^{ac} + l_{2a}^{ac}}{Bt_3}\right) - \frac{1}{h_{21}} f\left(\frac{l_{21}^{ac}}{Bt_3}\right) + \left(\frac{1}{h_{2a}} - \frac{1}{h_{21}}\right) f\left(\frac{l_{2a}^{ac}}{Bt_3}\right) \quad (24)$$

By combining this result with equation (20), the lemma is proven. \square

To address the nonconvexity of constraints (19c) and (19d), we introduce auxiliary variable ψ_1 and ψ_2 , where $\psi_1 = t_2\beta_1$, $\psi_2 = t_1\beta_2$ and $l_2^c = l_{21}^{ac} + l_{2a}^{ac}$. Additionally, based on Lemma 1, we replace the decision variables \mathbf{p} with \mathbf{l} and introduce decision variables set $\boldsymbol{\psi} = \{\psi_1, \psi_2\}$. We define $\mathbf{l}' = [l_{21}^b, l_{1a}^b, l_2^c, l_{2a}^c, l_{1a}^c]$ as the amount of task processing locally and offloading for both MD₁ and MD₂. Meanwhile, to simplify the mathematical expression, we denote some constants C_1, C_2, C_3 . $C_1 = \left(\frac{1}{h_{2a}} - \frac{1}{h_{21}}\right)$, $C_2 = \kappa_2\phi_2(f_2)^2$ and $C_3 = \kappa_1\phi_1(f_1)^2$. Therefore, sub-problem P2 can be transformed into problem P1.1.1, as follows:

$$(P2) : \min_{t, \boldsymbol{\psi}, \mathbf{l}'} P_0(t_0 + t_1 + t_2) \quad (25a)$$

$$\text{s.t. } t_0 + t_1 + t_2 + t_3 + t_4 \leq T \quad (25b)$$

$$P_2^b t_1 + \frac{t_3}{h_{21}} f\left(\frac{l_2^c}{Bt_3}\right) + t_3 C_1 f\left(\frac{l_{2a}^c}{Bt_3}\right) + C_2(L_2 - l_{21}^b - l_2^c) \quad (25c)$$

$$\leq \mu h_2 P_0(t_0 + t_2 + t_1 - \psi_2)$$

$$P_1^b t_2 + \frac{t_4}{h_{1a}} f\left(\frac{l_{1a}^c}{Bt_4}\right) + C_3(L_1 + l_{21}^b + l_2^c - l_{2a}^c - l_{1a}^b - l_{1a}^c) \quad (25d)$$

$$\leq \mu h_1 P_0(t_0 + t_2 + t_1 - \psi_1)$$

$$\frac{1}{h_{21}} f\left(\frac{l_2^c}{Bt_3}\right) + C_1 f\left(\frac{l_{2a}^c}{Bt_3}\right) \leq P_2^{\max} \quad (25e)$$

$$\frac{1}{h_{1a}} f\left(\frac{l_{1a}^c}{Bt_4}\right) \leq P_1^{\max} \quad (25f)$$

$$l_{21}^{ac} + l_{2a}^b \leq l_{1a}^b + l_{1a}^{ac} \quad (25g)$$

$$\frac{(L_2 - l_{21}^b - l_2^c)\phi_2}{f_2} \leq T - t_0 \quad (25h)$$

$$\frac{(L_1 + l_{21}^b + l_2^c - l_{2a}^c - l_{1a}^b - l_{1a}^c)\phi_1}{f_1} \leq T - t_0 \quad (25i)$$

$$0 \leq \psi_1 \leq t_2, 0 \leq \psi_2 \leq t_1 \text{ and (19j)} \quad (25j)$$

Problem P2 is a convex optimization problem according to the following Lemma.

Lemma 2. *Problem P2 is convex and can be efficiently solved using optimization tools such as CVX.*

Proof. First, the objective function is convex when P_0 is given. The constraints (25b), (25g), (25h), (25i) are linear inequalities, which are inherently convex.

Next, consider constraint (25c). The function $f\left(\frac{l_2^c}{B}\right)$ is convex, and its perspective $t_3 f\left(\frac{l_2^c}{Bt_3}\right)$ is also convex with respect to the variables l_2^c and t_3 , as the perspective operation preserve the convexity [43]. Similarly, the term $t_3 C_1 f\left(\frac{l_{2a}^c}{Bt_3}\right)$ is convex. Since the remaining terms in constraint (25c) are linear with respect to $t_1, l_{21}^b, l_2^c, t_0, t_2, \psi_2$, the entire constraint (25c) is convex. The same reasoning applies to constraint (25d), confirming its convexity.

For constraint (25e), the convexity is less straightforward. However, by multiplying both sides of the inequality by t_3 , we obtain:

$$t_3 \frac{1}{h_{21}} f\left(\frac{l_2^{ac}}{Bt_3}\right) + t_3 C_1 f\left(\frac{l_{2a}^{ac}}{Bt_3}\right) \leq t_3 P_2^{max} \quad (26)$$

In this inequation (26), $t_3 \frac{1}{h_{21}} f\left(\frac{l_2^{ac}}{Bt_3}\right)$ is convex with respect to l_2^{ac} and t_3 , as it represents the perspective of $f\left(\frac{l_2^{ac}}{Bt_3}\right)$. Similarly, $t_3 C_1 f\left(\frac{l_{2a}^{ac}}{Bt_3}\right)$ is convex with respect to l_{2a}^{ac} and t_3 . The term $t_3 P_2^{max}$ is linear in t_3 , making constraint (25e) a convex inequality. Using the same approach, we can confirm that constraint (25f) is also convex.

Therefore, Problem P2 is proved to be convex. \square

Besides, We use the Lagrange multiplier technique to derive valuable insights into the characteristics of the optimal solution.

Theorem 1. Given non-negative Lagrange multipliers λ_i , $i = 1, 2, \dots, 10$, the optimal power allocation $\mathbf{l} = [l_2^{ac}, l_{2a}^{ac}, l_{1a}^{ac}]$ must fulfill certain conditions

$$l_2^{ac,*} = \begin{cases} 0, & \text{if } t_3 = 0 \\ \left[Bt_3 \log_2 \left(\frac{-\lambda_7 \frac{\phi_2}{f_2} Bt_3 - \lambda_2 C_2 + \lambda_3 C_3 - \lambda_8 \frac{\phi_1}{f_1} Bt_3}{\lambda_2 \frac{t_3}{h_{21}} + \lambda_4 \frac{1}{h_{21}} \ln 2} \right) \right]^+, & \text{others} \end{cases} \quad (27a)$$

$$l_{2a}^{ac,*} = \begin{cases} 0, & \text{if } t_3 = 0 \\ \left[Bt_3 \log_2 \left(\frac{-\lambda_3 C_3 - \lambda_8 \frac{\phi_1}{f_1} Bt_3}{\lambda_2 C_1 \frac{t_3}{h_{21}} + \lambda_4 C_1 \frac{1}{h_{21}} \ln 2} \right) \right]^+, & \text{others} \end{cases} \quad (27b)$$

$$l_{1a}^{ac,*} = \begin{cases} 0, & \text{if } t_4 = 0 \\ \left[Bt_4 \log_2 \left(\frac{-\lambda_3 C_3 - \lambda_8 \frac{\phi_1}{f_1} Bt_4}{\lambda_3 \frac{t_4}{h_{1a}} + \lambda_5 \frac{1}{h_{1a}} \ln 2} \right) \right]^+, & \text{others} \end{cases} \quad (27c)$$

Proof. Let $\lambda_i \geq 0$ for $i = 1, 2, \dots, 10$ represent the Lagrange multipliers associated with the constraints. The Lagrangian function for problem (P1.1.1), formulated using these multipliers, is given by

$$\begin{aligned} L(\mathbf{t}, \boldsymbol{\psi}, \mathbf{l}') &= P_0(t_0 + t_1 + t_2) \\ &+ \lambda_1[t_0 + t_1 + t_2 + t_3 + t_4 - T] \\ &+ \lambda_2 \left[P_2^b t_1 + \frac{t_3}{h_{21}} f\left(\frac{l_2^{ac}}{Bt_3}\right) + t_3 C_1 f\left(\frac{l_{2a}^{ac}}{Bt_3}\right) + C_2(L_2 - l_{21}^b - l_2^{ac}) - \mu h_2 P_0(t_0 + t_2 + t_1 - \psi_2) \right] \\ &+ \lambda_3 \left[P_1^b t_2 + \frac{t_4}{h_{1a}} f\left(\frac{l_{1a}^{ac}}{Bt_4}\right) + C_3(L_1 + l_{21}^b + l_2^{ac} - l_{2a}^{ac} - l_{1a}^b - l_{1a}^{ac}) - \mu h_1 P_0(t_0 + t_2 + t_1 - \psi_1) \right] \\ &+ \lambda_4 \left[\frac{1}{h_{21}} f\left(\frac{l_2^{ac}}{Bt_3}\right) + C_1 f\left(\frac{l_{2a}^{ac}}{Bt_3}\right) - P_2^{max} \right] \\ &+ \lambda_5 \left[\frac{1}{h_{1a}} f\left(\frac{l_{1a}^{ac}}{Bt_4}\right) - P_1^{max} \right] \\ &+ \lambda_6 [l_{21}^{ac} + l_{2a}^b - l_{1a}^b + l_{1a}^{ac}] \\ &+ \lambda_7 \left[\frac{(L_2 - l_{21}^b - l_2^{ac})\phi_2}{f_2} - T - t_0 \right] \\ &+ \lambda_8 \left[\frac{(L_1 + l_{21}^b + l_2^{ac} - l_{2a}^{ac} - l_{1a}^b - l_{1a}^{ac})\phi_1}{f_1} - T - t_0 \right] \\ &+ \lambda_9[\psi_1 - t_2] \\ &+ \lambda_{10}[\psi_2 - t_1] \end{aligned} \quad (28)$$

We can use the first-order optimality conditions. Taking the derivative of the Lagrangian function yields

$$l_2^{ac,*} = \left[Bt_3 \log_2 \left(\frac{-\lambda_7 \frac{\phi_2}{f_2} Bt_3 - \lambda_2 C_2 + \lambda_3 C_3 - \lambda_8 \frac{\phi_1}{f_1} Bt_3}{\lambda_2 \frac{t_3}{h_{21}} + \lambda_4 \frac{1}{h_{21}} \ln 2} \right) \right]^+, \quad (29a)$$

$$l_{2a}^{ac,*} = \left[Bt_3 \log_2 \left(\frac{-\lambda_3 C_3 - \lambda_8 \frac{\phi_1}{f_1} Bt_3}{\lambda_2 C_1 \frac{t_3}{h_{21}} + \lambda_4 C_1 \frac{1}{h_{21}} \ln 2} \right) \right]^+, \quad (29b)$$

$$l_{1a}^{ac,*} = \left[Bt_4 \log_2 \left(\frac{-\lambda_3 C_3 - \lambda_8 \frac{\phi_1}{f_1} Bt_4}{\lambda_3 \frac{t_4}{h_{1a}} + \lambda_5 \frac{1}{h_{1a}} \ln 2} \right) \right]^+, \quad (29c)$$

By analyzing the first-order partial derivatives, we can determine the essential conditions for an optimal solution. Utilizing the connections between the auxiliary variables and the primary variables allows us to formulate the theorem. \square

According to this theorem, we can deduce that in the process of wireless radio frequency energy transfer, increasing the value of B will motivate MD_2 and MD_1 entities to offload data more, which correspondingly reduces the computational tasks they perform locally. Specifically, when $-\lambda_7 \frac{\phi_2}{f_2} Bt_3 - \lambda_2 C_2 + \lambda_3 C_3 - \lambda_8 \frac{\phi_1}{f_1} Bt_3 > \lambda_2 \frac{t_3}{h_{21}} + \lambda_4 \frac{1}{h_{21}} \ln 2$ the MD_2 is more inclined to offload tasks through the AT mode. For the MD_1 , a similar conclusion can be drawn.

The process of solving the original TEP problem, denoted as (P1), is encapsulated within Algorithm 1.

Algorithm 1: User-Assisted Dynamic Resource Allocation Algorithm

Input: the task arrival L_i ; the channel gain $\{h_i, g_{12}, g_{2a}\}$.

- 1 Variable substitution is conducted based on (20),(21),(24);
- 2 Calculate C_1, C_2, C_3 based on P1.1.1;
- 3 cvx_begin
- 4 Minimize P2
- 5 Subject to (25b)-(25j)
- 6 cvx_end
- 7 Calculate β^* based on $\psi_1 = t_2 \beta_1, \psi_2 = t_1 \beta_2$;
- 8 Calculate p^* based on (20),(21),(24);

Output: Obtain the optimal resource allocation $\{t^*, p^*, \beta^*, l^*\}$;

5.1. Algorithm Complexity Analysis

After transformation, the non-convex problem P1 is converted into a convex optimization problem P2, which involves a total of 12 variables. P2 can be solved using existing mature convex optimization algorithms, such as the interior-point method, with a time complexity of $O(n^{3.5} \log(1/\epsilon))$, where n is the number of decision variables. For P2, due to its small scale of variables, it can be solved quickly. Here we use the open-source cvx toolbox for solving it.

6. Simulation Results

In this section, we assess the performance of our proposed scheme through comprehensive numerical simulations. Our high-performance experimental setup, featuring a 2.10 GHz Intel(R) Xeon(R) Silver 4116 CPU and two GeForce RTX 4070 GPUs, ensures efficient simulation processing. We define the following parameters: A_d for antenna gain, f_c for carrier frequency, d_e for the path loss exponent, and d_i for the distance between nodes. We employ a free-space path loss model to simulate

signal propagation, with the average channel gain $\bar{h} = A_d \left(\frac{3 \times 10^8}{4\pi f_c d_i} \right)^{d_e}$. Additionally, we incorporate a Rayleigh fading model to account for channel gains. The simulation parameters are summarized in Table 2.

Table 2. SIMULATION PARAMETERS

Symbol	Value
Transmit power of the AP P_0	1 W
Bandwidth W	1.2 MHz
Noise power σ^2	10^{-3} W
The circuit consumption of the BackCom p_1^{ba} and p_2^{ba}	0.01 W
The distance between MD ₁ , MD ₂ and HAP	130 m, 180 m
The distance between MD ₁ and MD ₂	80 m
CPU frequency of MD ₁ f_1	250 MHz
CPU cycles to compute 1 bit task of MD ₁ ϕ_1	250 cycles/bit
CPU frequency of MD ₂ f_2	250 MHz
CPU cycles to compute 1 bit task of MD ₂ ϕ_2	150 cycles/bit
Equal computing efficiency parameter of MD ₁ κ_1	10^{-8}
Equal computing efficiency parameter of MD ₂ κ_2	10^{-8}
The antenna gain A_d	3
The carrier frequency f_c	915 Mhz
The path loss exponent d_e	3

To verify the performance of our proposed algorithm, we consider the following three representative benchmarks:

(1) UC With NOMA scheme [41]: By introducing NOMA technology without BackCom, MD₁ offloads tasks to MD₂ and HAP simultaneously.

(2) UC with BackCom scheme [10]: Users opt to complete computational tasks exclusively via the BackCom mode. Specifically, the HAP continuously broadcasts RF energy to the users throughout the time slot.

(3) Integrated BackCom and NOMA Without UC scheme [44]: The remote users directly offload computation tasks to the MEC server without the assistance of the nearby node.

Figure 2 illustrates the comparative analysis of energy consumption across different schemes under various latency constraint T , with parameters defined as $\zeta = -20$ dB, $p_0 = 1$ W, and $W = 1.2$ MHz. The results indicate a consistent decline in energy consumption for all four schemes, with our proposed algorithm demonstrating the lowest energy expenditure at any task processing latency constraints. Our proposed algorithm outperforms the other three schemes by reducing energy consumption by 20%, 40%, and 40% respectively when $T = 1$ s. From Figure 3, it can be observed that as the task execution delay constraint becomes tighter, our scheme achieves greater energy savings. Our algorithm outperforms the current state-of-the-art methods by approximately 8% under the same network configuration. This improvement underscores the algorithm's efficiency in energy utilization, as a result of effectively integrating multiple communication technologies, such as BackCom and NOMA.

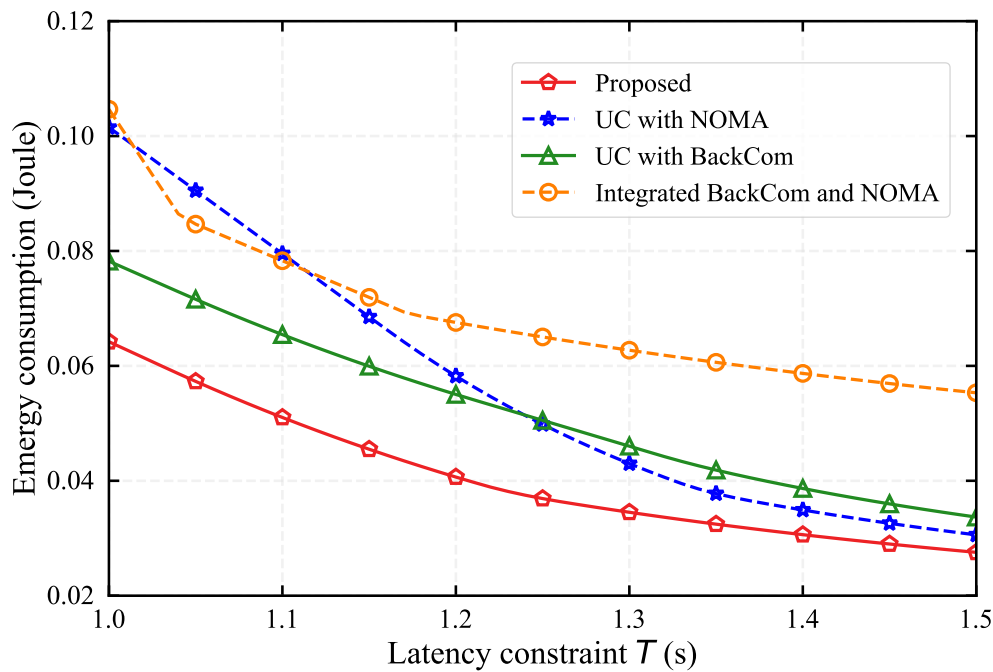


Figure 2. Energy consumption in different schemes versus the latency constraint T .

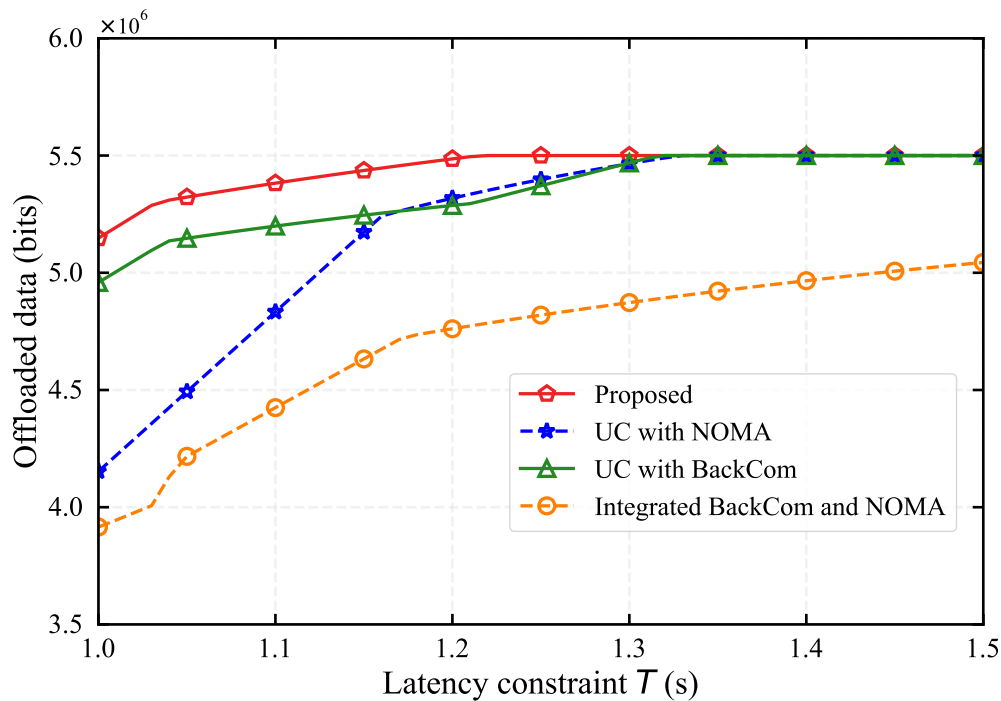


Figure 3. Offloaded data in different schemes versus the latency constraint T .

Figure 3 illustrates the amount of data processed by task offloading across various schemes with the latency constraint T ranging from 1.0 s to 1.5 s. The proposed algorithm is observed to consistently facilitate higher data offloading as the latency constraint T increases. It can be observed that the gap in offloaded data between the proposed algorithm and the other schemes widens when the latency constraint T is small, highlighting the algorithm's robustness and effectiveness under time-sensitive conditions. This trend indicates the algorithm's adeptness at managing task offloading within tight time constraints, suggesting the capability to utilize constraint resources in real-life scenarios. In

contrast, the without UC scheme, in which MD₁ directly offloads tasks to the HAP, suffers from the poor channel condition between MD₁ and HAP and exhibits the lowest data offloading capability.

Figure 4 illustrates the impact of input computation bits at MD₁ on energy consumption. It can be observed that our proposed algorithm achieves an average energy reduction of approximately 30% compared to other benchmark schemes. Notably, as the input computation bits escalate, the disparity in energy consumption between the proposed algorithm and the other three schemes becomes more pronounced. This divergence can be attributed to the algorithm's ability to optimize resource allocation and leverage advanced communication techniques, such as BackCom and NOMA, which become more beneficial under higher computational input. This experiment underscores the robustness of our proposed algorithm across various levels of input computation bits, suggesting its superior adaptability in diverse scenarios.

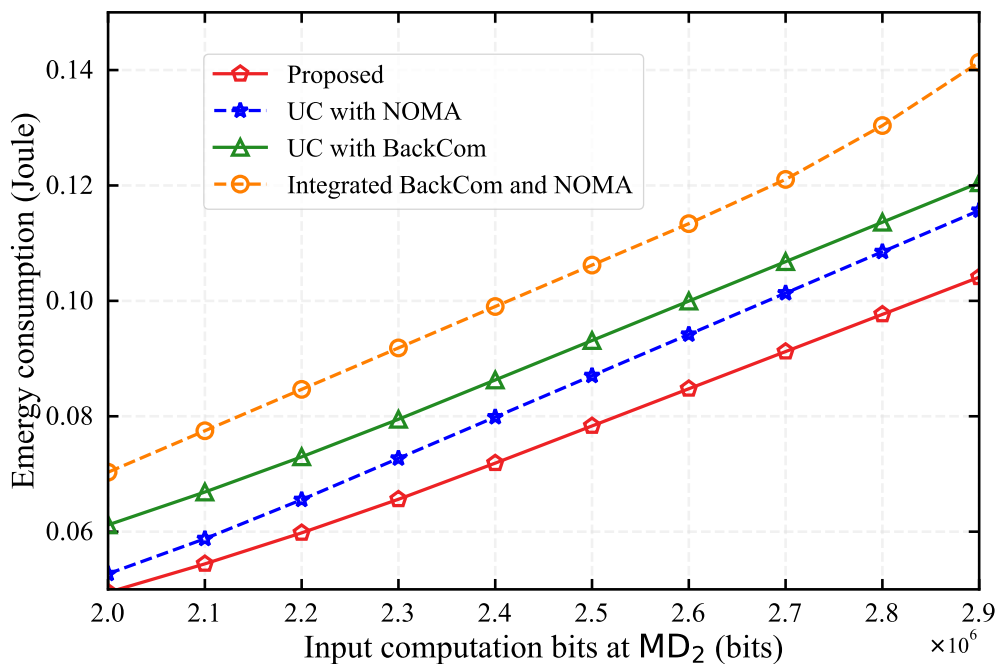


Figure 4. Energy consumption in different schemes versus input computation bits at MD₂.

Figure 5 illustrates the task offloading capabilities across four schemes. It is clear that the proposed algorithm consistently achieves the largest amount of data processed by task offloading, indicating its enhanced transmit capability. With an increase in the input computation bits, the performance gap between the proposed scheme and the benchmark schemes widens. The proposed algorithm demonstrates a notable advantage of 7%, 12%, and 17% over the other schemes. This advantage can be attributed to the integration of advanced communication techniques and the efficient allocation of resources. Furthermore, at an input computation bit value of 2.4 Mbits, the proposed algorithm reaches its peak performance, suggesting that an optimal balance has been achieved among the various communication techniques employed.

Figure 6 compares the energy consumption of four different algorithms under varying transmit power levels of the HAP, which in turn affects the energy harvested by MDs. It is evident that the our proposed algorithm consistently exhibits the lowest energy consumption of approximately 0.06 J across the entire spectrum of transmit power levels. The UC with BackCom scheme exhibits slightly higher energy consumption attributable to its less effective task offloading capability in the absence of NOMA's assistance. Moreover, the UC with NOMA and Integrated BackCom and NOMA without UC schemes demonstrates a steady decrease in energy consumption as the transmit power increases. This is because that their restricted transmission modes can not process enough tasks when energy is insufficient. This suggests that the proposed algorithm can adapts well to the variations in energy

supplies in different scenarios. The sub-optimal performance of benchmark schemes also indicates that the integration of BackCom and NOMA significantly enhances the energy efficiency and robustness of the system.

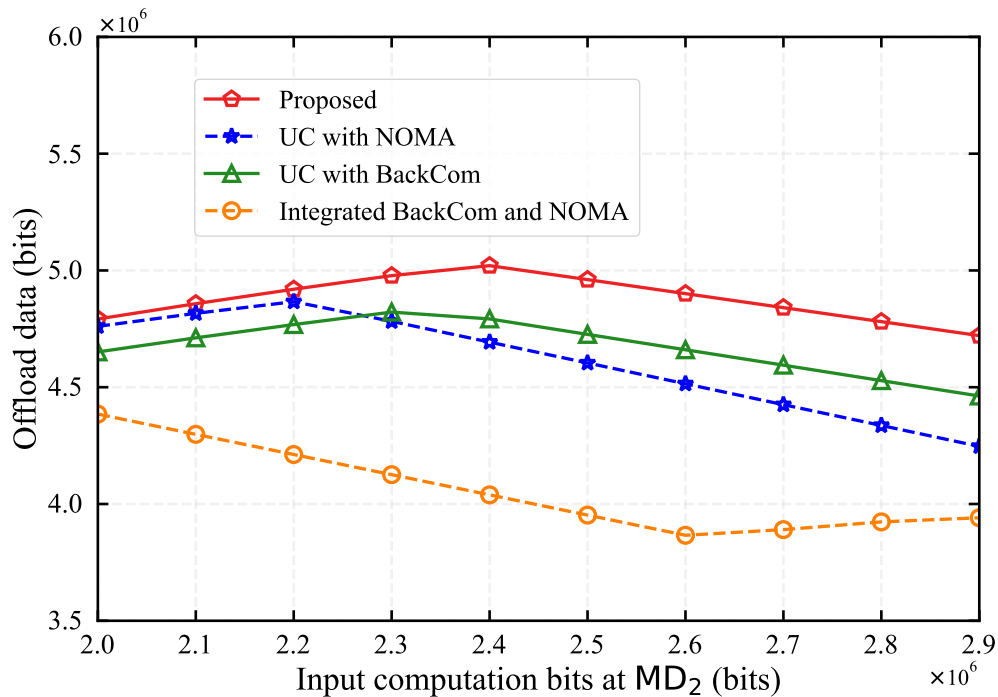


Figure 5. Offloaded data in different schemes versus input computation bits at MD₂.

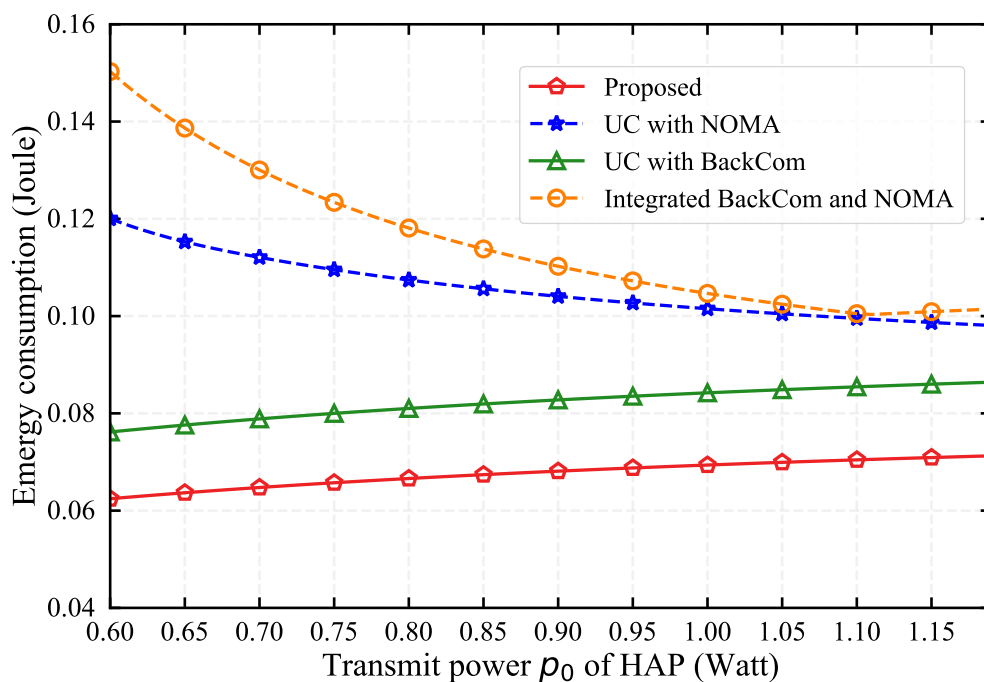


Figure 6. Energy consumption in different schemes versus transmit power p_0 of HAP.

Figure 7 compares the offloaded data of four schemes under different transmit power of the HAP. Notably, the proposed algorithm offloads largest amount of data whatever p_0 is, suggesting that MDs prefer to process tasks by task offloading. This is due to the strong task offloading capability

of the proposed algorithm, coming from the integrated communication techniques. The UC with BackCom, without NOMA technique, exhibits less favorable performance, with the UC with BackCom and Integrated BackCom and NOMA performing the worst. The Proposed UC with NOMA's ability to maintain high offloaded data levels even at lower power settings is particularly noteworthy. This indicates its robustness and adaptability, enabling efficient data offloading even under constrained energy conditions.

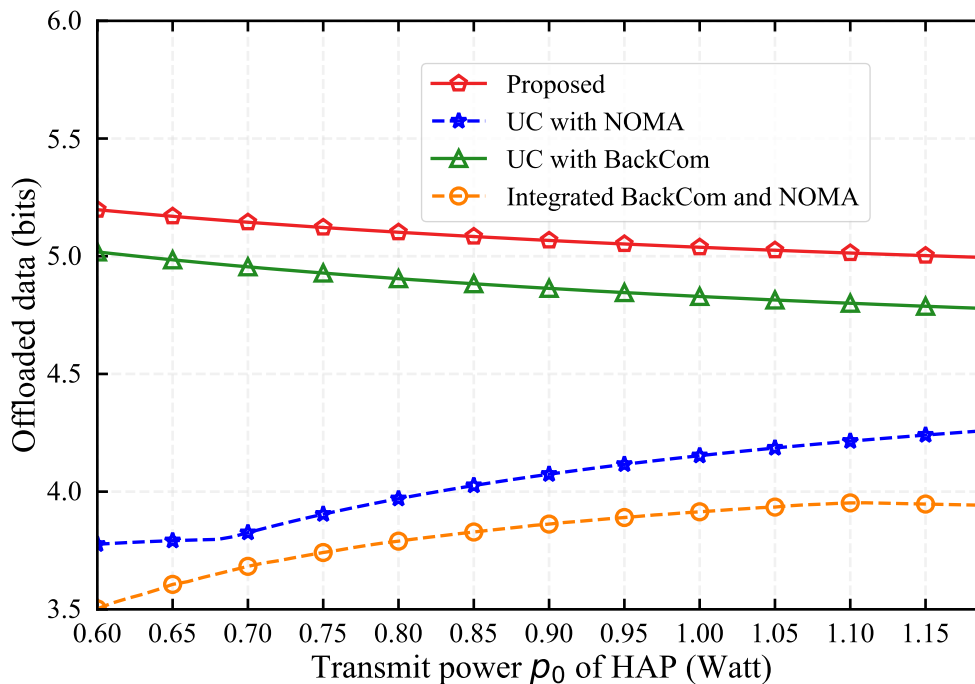


Figure 7. Offloaded data in different schemes versus transmit power p_0 of HAP.

In Figure 8, we evaluate the energy consumption of the four schemes under different offloading power constraint of MD₁. It is evident that the proposed algorithm consistently demonstrates the lowest energy consumption across the entire range of power constraints, indicating its superior efficiency. Interestingly, at lower power constraints for MD₁, the without UC with integrated BackCom and AC scheme performs extremely poorly. This underscores the critical role of user collaboration in energy-efficient task offloading. Meanwhile, the UC with BackCom scheme performs relatively better among benchmark schemes, suggesting that BackCom technology can significantly enhance task offloading efficiency when MD₁'s power is constrained. Overall, this simulation highlights the benefits of integrating multiple communication techniques, especially UC and BackCom, into the proposed algorithm.

Figure 9 illustrates the energy consumption patterns under varying distances between MD₁ and MD₂ from 50 to 110 meters. It is observed that the energy consumption for the proposed scheme, as well as the schemes incorporating UC with NOMA and UC with BackCom, all exhibit a decline as the distance grows. This decrease can be attributed to the reduction in channel gain with distance, which in turn requires more time and higher power to offload tasks, consequently increasing energy consumption. The scheme without UC but with integrated BackCom and NOMA does not show variation with distance, as it does not rely on task offloading between MD₁ and MD₂. This observation underscores the practical deployment consideration that the proper choice of helper devices should be maintained within an optimal range to prevent a sharp deterioration in network performance. The analysis not only quantifies the impact of distance on energy consumption but also highlights the critical role of user-cooperation in efficient network architectures.

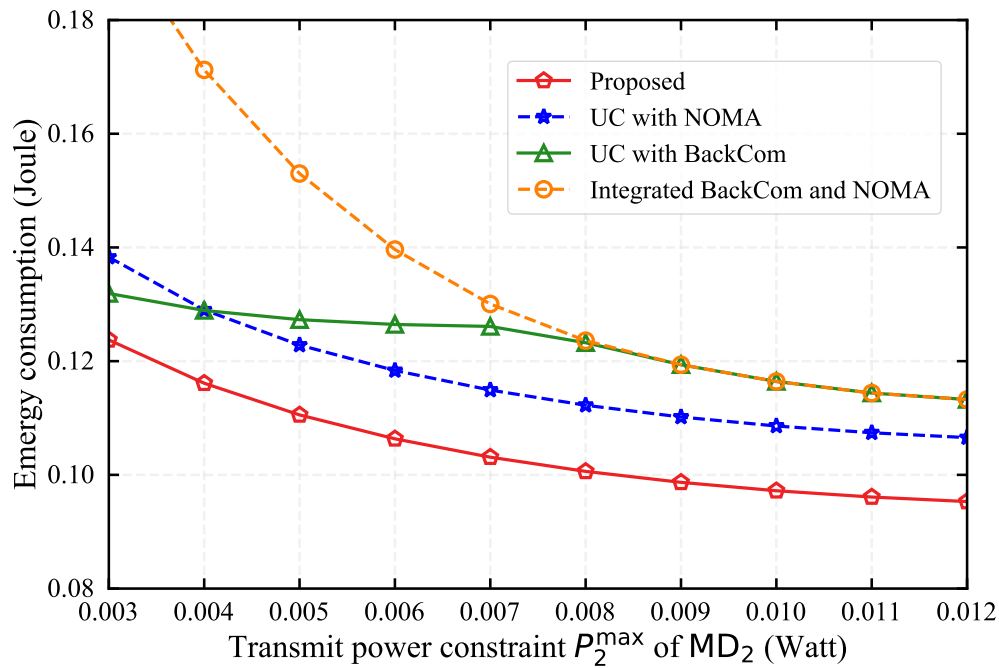


Figure 8. Energy consumption in different schemes versus transmit power constraint P_2^{\max} of MD_2 .

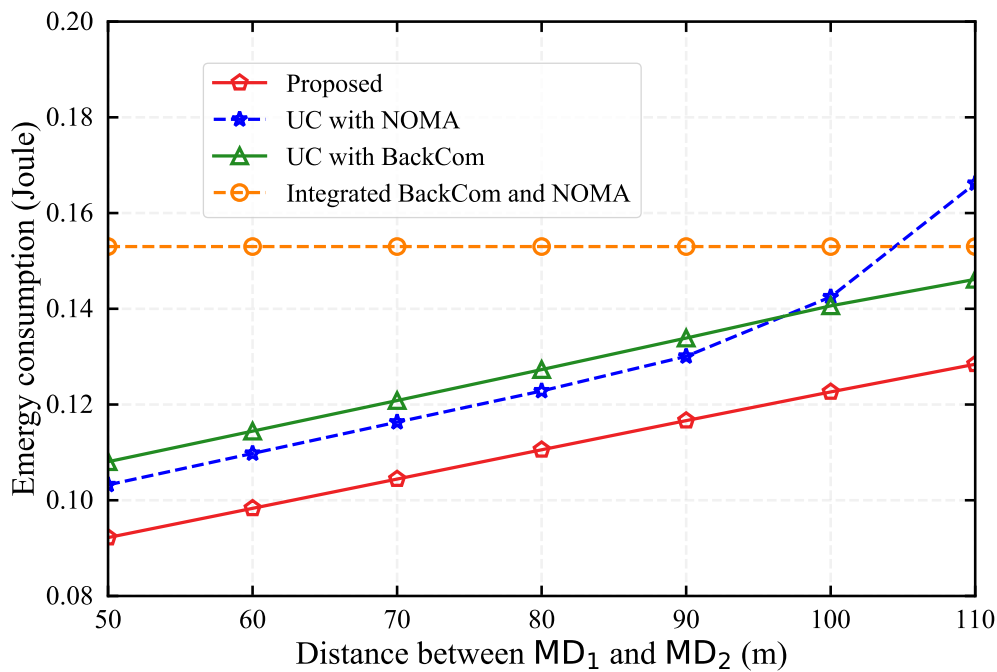


Figure 9. Energy consumption in different schemes versus the distance between MD_1 and MD_2 .

Figure 10 evaluates the task offloading strategy from MD_1 as the distance between MD_1 and MD_2 varies. As the distance between MD_1 and MD_2 increases, offloading tasks via UC to MD_2 becomes less efficient, prompting MD_1 to offload tasks directly to the HAP rather than relying on UC. This observation indicates that the proposed algorithm effectively adapts to network topological changes, such as the distance between mobile devices. By strategically diverting offloaded tasks to the HAP when UC is less efficient, the algorithm enhances overall network performance and minimizes energy consumption. In conclusion, the offloading strategy illustrated in Figure 10 demonstrates the algorithm's adaptability and efficiency in managing data flow, underscoring its capability to enhance network performance and energy efficiency in real-world scenarios.

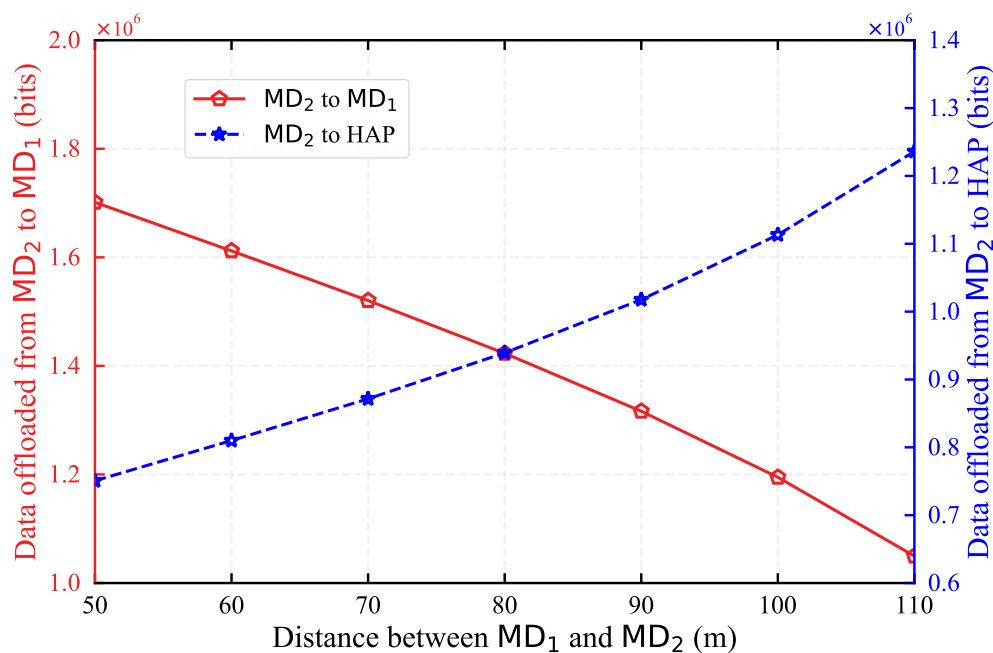


Figure 10. Offloading strategy under different distance between MD₁ and MD₂

7. Conclusions

This paper explores the strategy of using cooperative communication technology for computation offloading in a NOMA-WPMEC system. In this framework, the HAP provides power supply to user devices through wireless power transmission technology and acts as a mobile edge computing server to assist two mobile devices with different distances (near-end and far-end) in completing their computation-intensive and latency-sensitive tasks. We adopt a block-based "harvest-then-offload" protocol and allow for two offloading methods: BackCom and AC. In particular, the far-end device utilizes the NOMA protocol for task offloading when adopting the asynchronous computing mode. This study considers the joint allocation of time, resource allocation strategies, backscatter reflection coefficients, and power allocation for cooperative computation offloading, aiming to minimize the transmission energy required for the access point to complete the computing tasks of the two users. Simulation results prove that our proposed strategy significantly outperforms existing baseline schemes. Looking forward, our research will extend to configurations that include multiple edge nodes and helper nodes, in order to further enhance the flexibility and practicality of the system in a variety of real-world application environments.

Author Contributions: Methodology, H.H.; Validation, Z.C. and Y.Y.; Formal analysis, H.H.; Investigation, H.H. and H.F.; Resources, H.H.; Data curation, H.H. and S.H.; Writing—original draft, H.H. and H.F.; Writing—review and editing, H.H.; Supervision, D.Y. and H.H.; All authors have read and agreed to the published version of the manuscript.

Funding: This research was supported by the Science and Technology Planning Project of Guangdong Province, China (No.2021A0101180005), Science and Technology Development Fund of Macao (FDCT), Macao, China (#0033/2023/RIA1)

Institutional Review Board Statement: Not applicable

Informed Consent Statement: Not applicable

Data Availability Statement: Data are contained within the article.

Acknowledgments: We thank all of the reviewers for their valuable comments.

Conflicts of Interest: The authors declare no conflicts of interest.

References

1. Mi, X.; He, H.; Shen, H. A Multi-Agent RL Algorithm for Dynamic Task Offloading in D2D-MEC Network with Energy Harvesting. *Sensors* **2024**, *24*. doi:10.3390/s24092779.
2. Wang, X.; Li, J.; Ning, Z.; Song, Q.; Guo, L.; Guo, S.; Obaidat, M.S. Wireless powered mobile edge computing networks: A survey. *ACM Computing Surveys* **2023**, *55*, 1–37.
3. Ling, C.; Zhang, W.; He, H.; Yadav, R.; Wang, J.; Wang, D. QoS and Fairness Oriented Dynamic Computation Offloading in the Internet of Vehicles based on Estimate Time of Arrival. *IEEE Transactions on Vehicular Technology* **2024**.
4. Younis, A.; Maheshwari, S.; Pompili, D. Energy-Latency Computation Offloading and Approximate Computing in Mobile-Edge Computing Networks. *IEEE Transactions on Network and Service Management* **2024**.
5. Wei, Z.; Zhang, B.; Lin, S.; Wang, C. A self-oscillation WPT system with high misalignment tolerance. *IEEE Transactions on Power Electronics* **2023**.
6. Su, B.; Ni, Q.; Yu, W.; Pervaiz, H. Optimizing computation efficiency for NOMA-assisted mobile edge computing with user cooperation. *IEEE Transactions on Green Communications and Networking* **2021**, *5*, 858–867.
7. He, H.; Huang, F.; Zhou, C.; Shen, H.; Yang, Y. Maximizing Computation Rate for Sustainable Wireless-Powered MEC Network: An Efficient Dynamic Task Offloading Algorithm with User Assistance. *Mathematics* **2024**, *12*. doi:10.3390/math12162478.
8. Sun, M.; Xu, X.; Huang, Y.; Wu, Q.; Tao, X.; Zhang, P. Resource Management for Computation Offloading in D2D-Aided Wireless Powered Mobile-Edge Computing Networks. *Ieee Internet of Things Journal* **2021**, *8*, 8005–8020. doi:10.1109/jiot.2020.3041673.
9. Peng, J.; Qiu, H.; Cai, J.; Xu, W.; Wang, J. D2D-assisted multi-user cooperative partial offloading, transmission scheduling and computation allocating for MEC. *IEEE Transactions on Wireless Communications* **2021**, *20*, 4858–4873.
10. He, Y.; Wu, X.; He, Z.; Guizani, M. Energy efficiency maximization of backscatter-assisted wireless-powered MEC with user cooperation. *IEEE Transactions on Mobile Computing* **2023**, *23*, 1878–1887.
11. Li, Y.; Zhang, X.; Lei, B.; Zhao, Q.; Wei, M.; Qu, Z.; Wang, W. Computation Rate Maximization for Wireless Powered Edge Computing With Multi-User Cooperation. *IEEE Open Journal of the Communications Society* **2024**.
12. He, H.; Zhou, C.; Huang, F.; Shen, H.; Li, S. Energy-Efficient Task Offloading in Wireless-Powered MEC: A Dynamic and Cooperative Approach **2024**.
13. Liu, Z.; Qi, J.; Shen, Y.; Ma, K.; Guan, X. Maximizing energy efficiency in UAV-assisted NOMA-MEC networks. *IEEE Internet of Things Journal* **2023**.
14. Liu, P.; Wang, J.; Ma, K.; Guo, Q. Joint Cooperative Computation and Communication for Demand-Side NOMA-MEC Systems With Relay-Assisted in Smart Grid Communications. *IEEE Internet of Things Journal* **2024**.
15. Jiao, X.; Chen, Y.; Chen, Y.; Wu, X.; Guo, S.; Zhu, W.; Lou, W. SIC-Enabled Intelligent Online Task Concurrent Offloading for Wireless Powered MEC. *IEEE Internet of Things Journal* **2024**.
16. Gu, B.; Xu, Y.; Huang, C.; Hu, R.Q. Energy-efficient resource allocation for OFDMA-based wireless-powered backscatter communications. ICC 2021-IEEE International Conference on Communications. IEEE, 2021, pp. 1–6.
17. Xu, Y.; Gu, B.; Hu, R.Q.; Li, D.; Zhang, H. Joint computation offloading and radio resource allocation in MEC-based wireless-powered backscatter communication networks. *IEEE Transactions on Vehicular Technology* **2021**, *70*, 6200–6205.
18. Shi, L.; Ye, Y.; Chu, X.; Sun, S.; Lu, G. Energy-efficient resource allocation for backscatter-assisted wireless powered MEC. *IEEE Transactions on Vehicular Technology* **2023**, *72*, 9591–9596.
19. Gu, B.; Li, D.; Xie, H. Computation-Efficient Backscatter-Blessed MEC with User Reciprocity. *IEEE Transactions on Vehicular Technology* **2023**.
20. Ye, Y.; Shi, L.; Chu, X.; Hu, R.Q.; Lu, G. Resource allocation in backscatter-assisted wireless powered MEC networks with limited MEC computation capacity. *IEEE Transactions on Wireless Communications* **2022**, *21*, 10678–10694.

21. Wu, T.; He, H. An Efficient Energy Efficiency Maximization Algorithm for Backscatter-Assisted WP-MEC Network with Relay. *Proceedings of the 2024 16th International Conference on Machine Learning and Computing*, 2024, pp. 720–727.
22. Li, X.; Zhao, M.; Zeng, M.; Mumtaz, S.; Menon, V.G.; Ding, Z.; Dobre, O.A. Hardware impaired ambient backscatter NOMA systems: Reliability and security. *IEEE Transactions on Communications* **2021**, *69*, 2723–2736.
23. Chen, W.; Ding, H.; Wang, S.; da Costa, D.B.; Gong, F.; Nardelli, P.H.J. Backscatter cooperation in NOMA communications systems. *IEEE Transactions on Wireless Communications* **2021**, *20*, 3458–3474.
24. Asif, M.; Ihsan, A.; Khan, W.U.; Ranjha, A.; Zhang, S.; Wu, S.X. Energy-efficient backscatter-assisted coded cooperative NOMA for B5G wireless communications. *IEEE Transactions on Green Communications and Networking* **2022**, *7*, 70–83.
25. Ahmed, M.; Shahwar, M.; Khan, F.; Khan, W.U.; Ihsan, A.; Khan, U.S.; Xu, F.; Chatzinotas, S. NOMA-Based Backscatter Communications: Fundamentals, Applications, and Advancements. *IEEE Internet of Things Journal* **2024**.
26. Van Nguyen, M.S.; Do, D.T.; Vahid, A.; Muhaidat, S.; Sicker, D. Enhancing NOMA backscatter IoT communications with RIS. *IEEE Internet of Things Journal* **2023**.
27. Mach, P.; Becvar, Z. Mobile edge computing: A survey on architecture and computation offloading. *IEEE communications surveys & tutorials* **2017**, *19*, 1628–1656.
28. Zhang, K.; Leng, S.; He, Y.; Maharjan, S.; Zhang, Y. Mobile edge computing and networking for green and low-latency Internet of Things. *IEEE Communications Magazine* **2018**, *56*, 39–45.
29. Dinh, T.Q.; Tang, J.; La, Q.D.; Quek, T.Q. Offloading in mobile edge computing: Task allocation and computational frequency scaling. *IEEE Transactions on Communications* **2017**, *65*, 3571–3584.
30. Wang, Y.; Chen, M.; Li, Z.; Hu, Y. Joint allocations of radio and computational resource for user energy consumption minimization under latency constraints in multi-cell MEC systems. *IEEE Transactions on Vehicular Technology* **2022**, *72*, 3304–3320.
31. Mei, J.; Dai, L.; Tong, Z.; Zhang, L.; Li, K. Lyapunov optimized energy-efficient dynamic offloading with queue length constraints. *Journal of Systems Architecture* **2023**, *143*, 102979.
32. Chen, M.; Liu, W.; Wang, T.; Zhang, S.; Liu, A. A game-based deep reinforcement learning approach for energy-efficient computation in MEC systems. *Knowledge-Based Systems* **2022**, *235*, 107660.
33. Ding, Z.; Poor, H.V. Advantages of NOMA for multi-user BackCom networks. *IEEE Communications Letters* **2021**, *25*, 3408–3412.
34. Khan, W.U.; Ihsan, A.; Nguyen, T.N.; Ali, Z.; Javed, M.A. NOMA-enabled backscatter communications for green transportation in automotive-industry 5.0. *IEEE Transactions on Industrial Informatics* **2022**, *18*, 7862–7874.
35. Toro, U.S.; Wu, K.; Leung, V.C. Backscatter wireless communications and sensing in green Internet of Things. *IEEE Transactions on Green Communications and Networking* **2021**, *6*, 37–55.
36. Shi, L.; Ye, Y.; Chu, X.; Lu, G. Computation bits maximization in a backscatter assisted wirelessly powered MEC network. *IEEE Communications Letters* **2020**, *25*, 528–532.
37. Fang, F.; Wang, K.; Ding, Z.; Leung, V.C. Energy-efficient resource allocation for NOMA-MEC networks with imperfect CSI. *IEEE Transactions on Communications* **2021**, *69*, 3436–3449.
38. Shi, J.; Zhou, Y.; Li, Z.; Zhao, Z.; Chu, Z.; Xiao, P. Delay minimization for NOMA-mmW scheme-based MEC offloading. *IEEE Internet of Things Journal* **2022**, *10*, 2285–2296.
39. Sun, Y.; Xu, J.; Cui, S. User association and resource allocation for MEC-enabled IoT networks. *IEEE Transactions on Wireless Communications* **2022**, *21*, 8051–8062.
40. Lyu, B.; Hoang, D.T.; Yang, Z. User cooperation in wireless-powered backscatter communication networks. *IEEE Wireless Communications Letters* **2019**, *8*, 632–635.
41. Huang, Y.; Liu, Y.; Chen, F. NOMA-aided mobile edge computing via user cooperation. *IEEE Transactions on Communications* **2020**, *68*, 2221–2235.
42. Verdu, S. Fifty years of Shannon theory. *IEEE Transactions on information theory* **1998**, *44*, 2057–2078.

43. Vandenberghe, L.; Boyd, S. *Convex optimization*; Vol. 1, Cambridge university press Cambridge, 2004.
44. Shi, L.; Ye, Y.; Chu, X.; Lu, G. Computation Bits Maximization in a Backscatter Assisted Wirelessly Powered MEC Network. *IEEE Communications Letters* **2021**, *25*, 528–532. doi:10.1109/LCOMM.2020.3027294.

Disclaimer/Publisher's Note: The statements, opinions and data contained in all publications are solely those of the individual author(s) and contributor(s) and not of MDPI and/or the editor(s). MDPI and/or the editor(s) disclaim responsibility for any injury to people or property resulting from any ideas, methods, instructions or products referred to in the content.